Neuron
Article

An Epilepsy/Dyskinesia-Associated Mutation Enhances BK Channel Activation by Potentiating Ca^{2+} Sensing

Junqiu Yang,[1,2,7] Gayathri Krishnamoorthy,[1,3,7] Akansha Saxena,[4,5,7] Guohui Zhang,[1,5] Jingyi Shi,[1,5] Huanghe Yang,[1,5] Kelli Delaloye,[1,5] David Sept,[4,5,6,*] and Jianmin Cui[1,5,*]
[1]Cardiac Bioelectricity and Arrhythmia Center, Washington University, St Louis, MO 63130, USA
[2]Department of Energy, Environmental, and Chemical Engineering, Washington University, St Louis, MO 63130, USA
[3]Department of Biomedical Engineering, Case Western Reserve University, Cleveland, OH 44106, USA
[4]Center for Computational Biology, Washington University, St Louis, MO 63130, USA
[5]Department of Biomedical Engineering, Washington University, St Louis, MO 63130, USA
[6]Present address: Department of Biomedical Engineering and Center for Computational Medicine and Bioinformatics, University of Michigan, Ann Arbor, MI 48109, USA
[7]These authors contributed equally to this work
*Correspondence: dsept@umich.edu (D.S.), jcui@biomed.wustl.edu (J.C.)
DOI 10.1016/j.neuron.2010.05.009

SUMMARY

Ca^{2+}-activated BK channels modulate neuronal activities, including spike frequency adaptation and synaptic transmission. Previous studies found that Ca^{2+}-binding sites and the activation gate are spatially separated in the channel protein, but the mechanism by which Ca^{2+} binding opens the gate over this distance remains unknown. By studying an Asp-to-Gly mutation (D434G) associated with human syndrome of generalized epilepsy and paroxysmal dyskinesia (GEPD), we show that a cytosolic motif immediately following the activation gate S6 helix, known as the AC region, mediates the allosteric coupling between Ca^{2+} binding and channel opening. The GEPD mutation inside the AC region increases BK channel activity by enhancing this allosteric coupling. We found that Ca^{2+} sensitivity is enhanced by increases in solution viscosity that reduce protein dynamics. The GEPD mutation alters such a response, suggesting that a less flexible AC region may be more effective in coupling Ca^{2+} binding to channel opening.

INTRODUCTION

Ion channels are proteins that conduct ions across cell membranes. Channel proteins regulate membrane excitation and ionic homeostasis in response to cellular signals, and mutations of ion channels often induce serious, sometimes life-threatening, diseases (Ashcroft, 2000). Structural studies in recent years have greatly advanced our understanding of the basic working modules of ion channels, including the activation gate (Yellen, 1998) and sensors to various stimuli such as voltage (Bezanilla, 2008; Swartz, 2008) and chemical ligands (Jiang et al., 2002; Unwin, 2003; Xia et al., 1998; Zagotta et al., 2003). However, the structural basis for the energetic coupling between sensors and the activation gate still remains elusive. Considering the fact that many disease-causing mutations are outside of the gate and sensors, it is particularly important to understand the molecular mechanism of the energetic coupling (i.e., the structural components of the allosteric activation pathways) and how they are modified by channel mutations. Activated by both membrane depolarization and increases in intracellular Ca^{2+} concentration ($[Ca^{2+}]_i$), large-conductance, voltage and calcium-activated K^+ (BK) channels become one of the best systems to address this question (Cui et al., 2009). Recently, we characterized a mutation D434G in human BK channels (hSlo1, GenBank accession number, GI: 26638649) that was identified from patients with nervous disorders of coexistent generalized epilepsy and paroxysmal dyskinesia (Du et al., 2005). This epilepsy/dyskinesia mutation (hD434G) significantly increases Ca^{2+} sensitivity of BK channels under physiological conditions. More interestingly, the hD434G mutation resides in a cytosolic motif, which is important for the allosteric coupling between Ca^{2+} binding and channel activation (Jiang et al., 2002; Krishnamoorthy et al., 2005), but outside of the putative Ca^{2+}-binding sites (Figure 1A), implying its role in the allosteric Ca^{2+}-dependent activation. Thus, this mutation provides us with a unique opportunity to uncover the structural basis and dynamic nature of the coupling between Ca^{2+} binding and BK channel opening.

BK channels are composed of four identical alpha subunits encoded by the *Slo1* gene (Atkinson et al., 1991; Shen et al., 1994). Each Slo1 subunit contains a membrane-spanning domain, which includes the voltage sensor and the ionic pore with the activation gate, and a large cytoplasmic C-terminal domain where two putative Ca^{2+}-binding sites, D367 and the Ca^{2+} bowl, have been identified (Schreiber and Salkoff, 1997; Xia et al., 2002) (Figure 1A). In addition, the channel contains a third site that binds both Ca^{2+} and Mg^{2+} at high (mM) concentrations (Shi et al., 2002; Xia et al., 2002; Yang et al., 2008), which is not shown in Figure 1A because, under the experimental conditions used in this study, this site will not be occupied. The atomic structure of the BK channel has not been solved. However, the

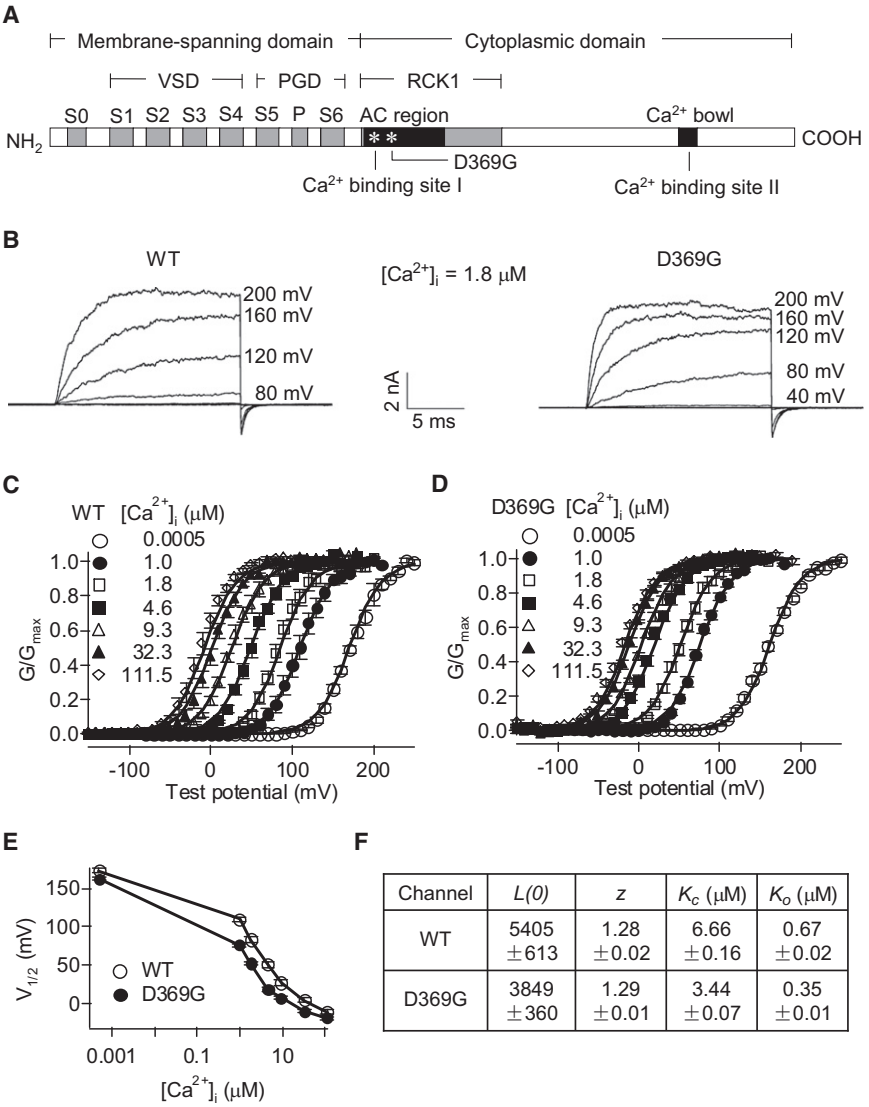

Channel	*L(0)*	*z*	K_c (μM)	K_o (μM)
WT	5405 ±613	1.28 ±0.02	6.66 ±0.16	0.67 ±0.02
D369G	3849 ±360	1.29 ±0.01	3.44 ±0.07	0.35 ±0.01

Figure 1. The Epilepsy/Dyskinesia Mutation mD369G Enhances Ca^{2+} Sensitivity of mSlo1 BK Channel Activation

(A) The Slo1 polypeptide. The membrane-spanning domain contains helices S0-S6 and pore loop (P), of which S1-S4 form the voltage sensor domain (VSD) and S5-S6 form the pore/gate domain (PGD). The cytoplasmic domain contains two putative Ca^{2+}-binding sites: the D367 site (Site I) and the Ca^{2+} bowl (Site II). mD369G is located in the AC region, close to the D367 Ca^{2+}-binding site.

(B) Macroscopic current traces from inside-out patches expressing WT and mD369G channels. Currents were elicited in 1.8 μM $[Ca^{2+}]_i$ by voltages as indicated. The voltages before and after the pulses were −50 mV.

(C and D) G-V curves for WT and mD369G channels in $[Ca^{2+}]_i$ from nominal 0 (~0.5 nM) to 111.5 μM. Solid lines are fits with the MWC model (see Experimental Procedures).

(E) $V_{1/2}$ of G-V curves versus $[Ca^{2+}]_i$ for WT and mD369G channels.

(F) Parameters of MWC model fits for WT and mD369G channels (value ± standard deviation). Error bars represent SEM.

X-ray crystallographic structure of $K_V1.2$ channel (Long et al., 2005) has been used as a model for the membrane-spanning domain of BK channels, whereas the RCK (regulator of K^+ conductance) domains of the MthK channel (Jiang et al., 2002) are suggested as a model for the cytoplasmic domain (Cui et al., 2009). A recent three-dimensional structure of BK channels from electron cryomicroscopy is consistent with these homology models (Wang and Sigworth, 2009). Structural and functional studies suggested that Ca^{2+} binding activates the channel through an allosteric mechanism (Magleby, 2003). At the molecular level, the allosteric mechanism is suggested to be similar to that for the MthK channel such that Ca^{2+} binding first alters the conformation of the cytosolic domain, which then opens the activation gate by pulling the S6 transmembrane segment (Jiang et al., 2002; Niu et al., 2004). To date, no structural component in the cytosolic domain that changes conformation during Ca^{2+}-dependent activation has been identified in BK channels, and the nature of such conformational changes is not known. The hD434G mutation in BK channels causes an increase in the activity of BK channels at the same membrane potentials and in $[Ca^{2+}]_i$ as compared to the wild-type (WT) hSlo1 channels. This change may be the basis for the association of the mutation with the neurological disorders (Brenner et al., 2005; Du et al., 2005). To investigate how this mutation uniquely enhances channel function, we studied the hD434G-equivalent D369G in mouse Slo1 (mSlo1) BK channels (Figure 1). These studies identified the N terminus of the RCK1 domain containing 76 amino acids, a region including the secondary structures βA-αC (Jiang et al., 2002) and thus named the AC region, as part of a structural basis connecting Ca^{2+} binding to channel opening. The results suggested a conformational and dynamical change of the AC region during BK channel activation that is altered by the mD369G mutation. These results also provide a novel allosteric mechanism for how ligand binding opens activation gates in ion channels.

RESULTS

mD369G Enhances Ca^{2+}-Dependent Activity

Experiments were performed on mSlo1 rather than hSlo1. The mSlo1 channel is homologous to hSlo1; aside from the different lengths at the N and C termini, 99% of amino acids are identical between the two channels (Butler et al., 1993; Du et al., 2005). The D369G mSlo1 channels exhibit the same phenotype as D434G hSlo1 such that, at the same voltage and physiological

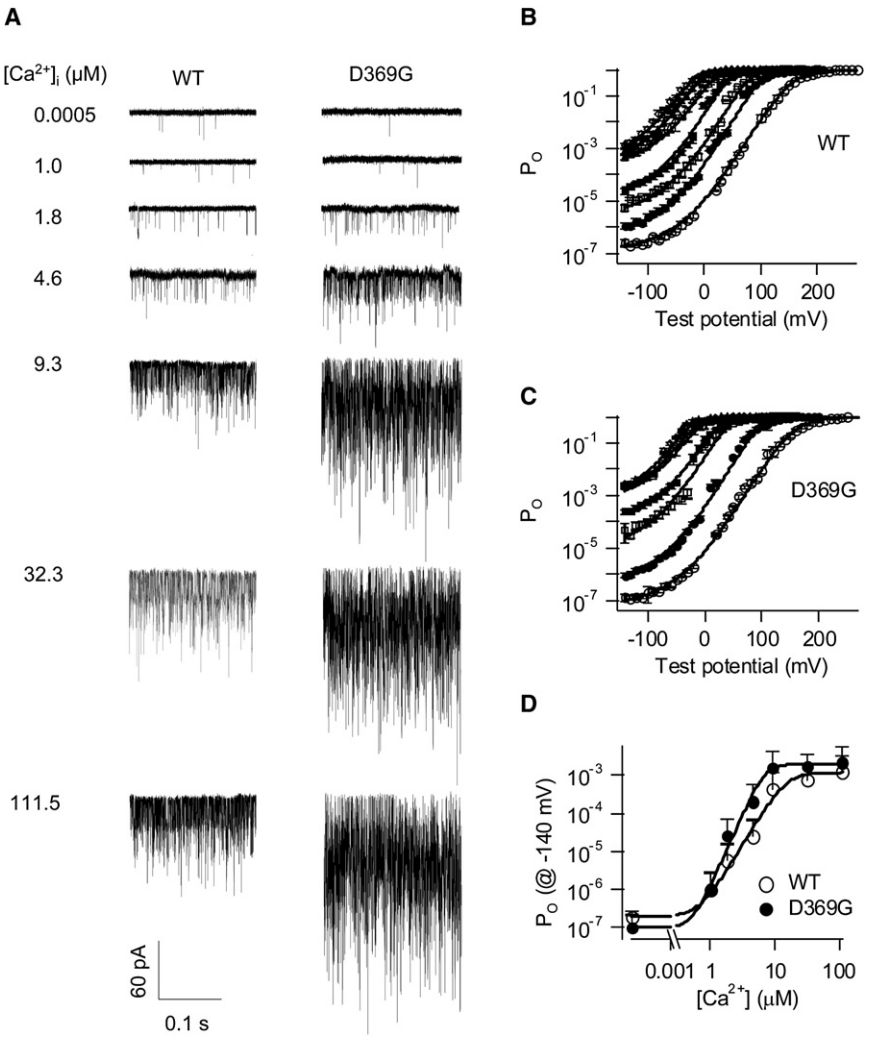

Figure 2. mD369G Enhances Ca^{2+} Sensitivity as Shown by Limiting Slope Measurement

(A) Current traces at −140 mV under different $[Ca^{2+}]_i$ for WT and mD369G. The patch for WT has ~730 channels, and the one for mD369G has ~550 channels. $[Ca^{2+}]_i$ is labeled next to the corresponding traces.

(B and C) P_o-V relations for WT (B) and mD369G (C) under different $[Ca^{2+}]_i$. The symbols for each $[Ca^{2+}]_i$ are identical to Figures 1C and 1D. Solid lines are fittings to the HCA model. Error bars represent SEM.

(D) P_o at −140 mV under different $[Ca^{2+}]_i$ for WT and mD369G. Solid lines are fittings to the Hill equation: $P_o = 1/(1+(K_A/[Ca^{2+}])^n)$. The microscopic dissociation constant K_A = 15 and 8 μM and the Hill coefficient n = 2.8 and 3.5 for WT and mD369G, respectively. Error bars represent SD of fitting.

$[Ca^{2+}]_i$, the mutant channels activated more than the WT channels (Figure 1B). We studied the mSlo1 channels over a more complete range of $[Ca^{2+}]_i$ from nominal 0 (~0.5 nM) to the near saturating 111.5 μM, and the results revealed that the mutation enhances Ca^{2+} sensitivity of channel activation (Figures 1C–1F). The increase of $[Ca^{2+}]_i$ shifted the voltage range of the conductance-voltage (G-V) relations of the mutant channels to more negative voltages as compared to those of the WT channels (Figures 1C and 1D). The G-V relation of BK channel activation can be approximated by fitting the data to the Boltzmann function with two independent parameters: $V_{1/2}$ (voltage at half-maximum conductance) and z (proportional to the steepness of the curve). A plot of $V_{1/2}$ versus $[Ca^{2+}]_i$ clearly shows that Ca^{2+} binding shifts the G-V relation to more negative voltage ranges, and that the shifts for the mD369G mutant channels are larger than that for the WT channels (Figure 1E). To further quantitatively estimate the change of Ca^{2+} sensitivity caused by the mutation, we fit the G-V relations of both mutant and WT channels at various $[Ca^{2+}]_i$ to the MWC model of BK channel activation (Cox et al., 1997; Magleby, 2003) (Figures 1C and D) and list the parameters (Figure 1F), where K_o and K_c are dissociation constants for Ca^{2+} binding at the open and closed conformations, respectively. The mD369G mutation decreased both K_o and K_c, consistent with an enhancement of Ca^{2+} sensitivity. Such a change in Ca^{2+} sensitivity would increase open probability of the channel by 1.4–5 times during a neuronal action potential with an estimated amplitude of ~30 mV and local $[Ca^{2+}]_i$ between 2 and 10 μM (Figures 1C and 1D). Previous studies suggested that the increased BK channel activity may be prominent at the peak of neuronal action potentials, where $[Ca^{2+}]_i$ increases as a result of Ca^{2+} influx via voltage-dependent Ca^{2+} channels, to reduce the duration and increase the frequency of action potentials and result in seizures (Brenner et al., 2005).

The shift of G-V relations in response to changes in $[Ca^{2+}]_i$ is an effective measurement of Ca^{2+} sensitivity of BK channels (Cui et al., 1997), which has been the primary method for investigating the gating mechanism of BK channels, including the identification of Ca^{2+}-binding sites (Schreiber et al., 1999; Xia et al., 2002). However, because BK channels are activated by both voltage and Ca^{2+} (Cui et al., 2009), this method does not directly reveal the mechanistic properties of Ca^{2+}-dependent activation. To eliminate the influence of voltage-dependent activation, we further examined Ca^{2+} sensitivities of the WT and D367G mSlo1 using limiting slope measurements at extremely negative voltages where BK channels open spontaneously and independently of voltage sensor movements (Horrigan et al., 1999). A patch containing hundreds of BK channels is held at negative voltages, where the open probability of the channels is so small that only rare openings of single channels are observed (Figure 2A). The open probability of the channels increases in the presence of Ca^{2+}, resulting in marked increase of single channel openings. Figure 2 shows that mutation mD369G

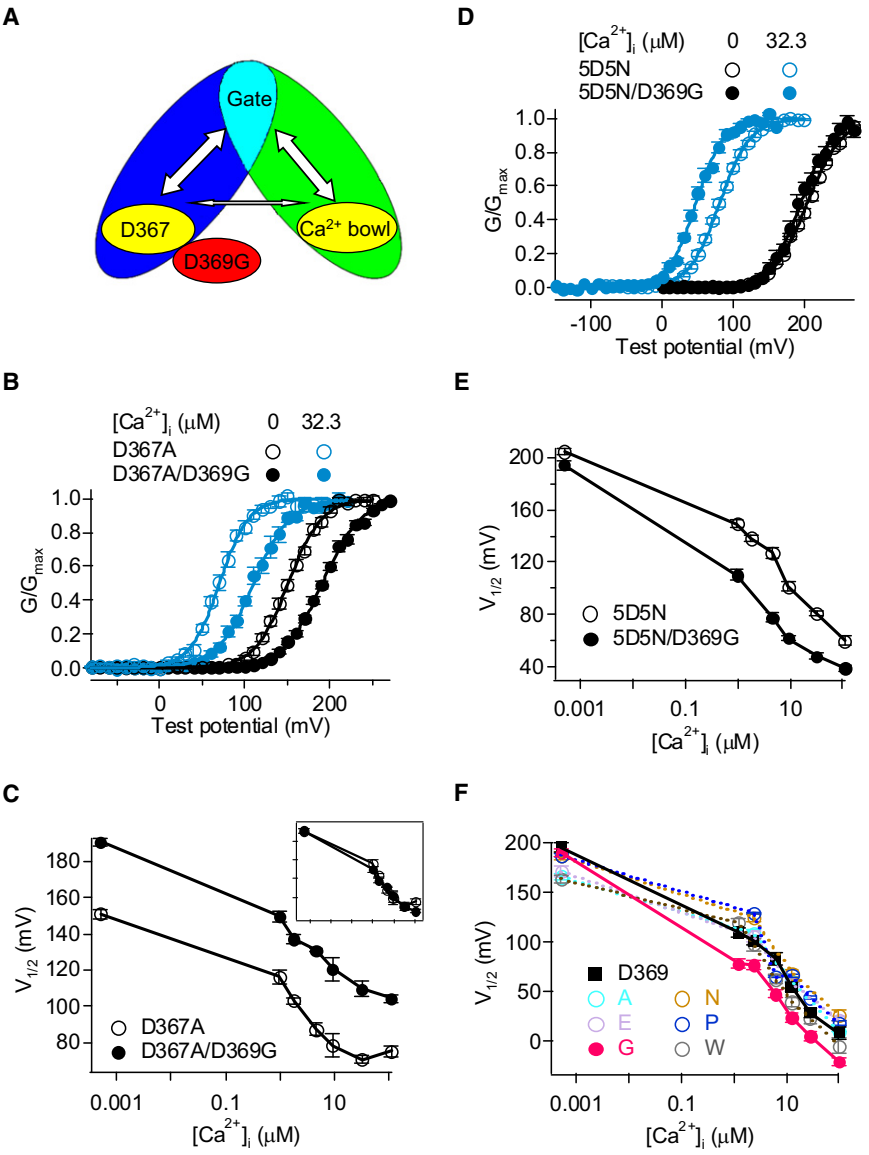

Figure 3. mD369G Mutation Specifically Affects the D367-Associated Ca^{2+} Activation Pathway

(A) Diagram illustrating the relationship between Ca^{2+}-binding sites and the gate. Ca^{2+} binding to the two sites, which are located distant from the activation gate, activates the channel through independent pathways with little cooperativity. mD369G is located close to the D367 site.

(B and D) G-V curves for D367A and D367A/D369G mutants (B) and for 5D5N and 5D5N/D369G mutants (D) with 0 and 32.3 μM $[Ca^{2+}]_i$. Solid lines are fits with the Boltzmann function.

(C and E) $V_{1/2}$ versus $[Ca^{2+}]_i$ for D367A and D367A/D369G mutants (C) and for 5D5N and 5D5N/D369G mutants (E). The curves for D367A and D367A/D369G are shifted vertically to align at 0 $[Ca^{2+}]_i$ in the inset of (C).

(F) $V_{1/2}$ versus $[Ca^{2+}]_i$ for WT and D369A, E, G, N, P, and W mutants. Note that the data in this panel were obtained in a different batch of experiments with a different set of Ca^{2+} solutions; hence, the final Ca^{2+} concentrations are slightly different from those in other figures.

Error bars represent SEM.

enhances Ca^{2+} sensitivity of the channel. At −140 mV, the number of single channel opening events of both WT and mD369G increases with increasing $[Ca^{2}]_i$, but more prominently for mD369G (Figure 2A). The P_o-V relations at various $[Ca^{2}]_i$ become flat at negative voltages (Figures 2B and 2C), indicating that channel opening at these voltages no longer depends on voltage sensor movements. The Ca^{2+} dependences of P_o at −140 mV for WT and mD369G channels (Figure 2D) clearly show that mutation mD369G enhances Ca^{2+} sensitivity. The fit of the data by the Hill equation (solid lines) results in a microscopic dissociation contant of 15 and 8 μM and a Hill coefficient of 2.8 and 3.5 for WT and mD369G, respectively. The larger Hill coefficient for mD369G indicates a higher cooperativity among Ca^{2+}-binding sites in the mD369G channels; thus, mutation mD369G enhances the allosteric coupling among Ca^{2+}-binding sites, possibly via an enhanced allosteric coupling between Ca^{2+}-binding sites and the activation gate.

mD369G Alters the D367 Activation Pathway

How does the mD369G mutation perturb the molecular mechanism of Ca^{2+}-dependent activation to result in a gain-of-function? Previous studies showed that the mutation of each of the two putative Ca^{2+}-binding sites, D367A and 5D5N (five consecutive Asp residues at 897–901 mutated to Asn), eliminates part of Ca^{2+}-dependent activation and that the sum of the effects is close to the total high-affinity Ca^{2+} sensitivity of the channel. These results suggest that the channel is activated by two separate Ca^{2+}-dependent pathways involving either D367 or the Ca^{2+} bowl, with only a weak cooperativity between the two pathways (Qian et al., 2006; Sweet and Cox, 2008; Xia et al., 2002) (Figure 3A). Therefore, to answer the above question, we first investigated whether the mD369G mutation affects each of the activation pathways and then addressed how a particular pathway is affected. We found that eliminating the function of one pathway by D367A also abolishes the difference in Ca^{2+}-induced G-V shift between the mD369G mutant and the WT channels, since $V_{1/2}$ changes with $[Ca^{2+}]_i$ nearly in parallel for the two channels (Figures 3B and 3C). This result indicates that the mD369G mutation no longer enhances Ca^{2+} sensitivity when the pathway associated with D367 is disabled. On the contrary, when the function of the Ca^{2+} bowl pathway is eliminated by the 5D5N mutation, the mD369G

mutation continues to enhance Ca^{2+} sensitivity in a similar way as in the WT channel (Figures 3D and 3E). Taken together, these results suggest that the epilepsy/dyskinesia mutation specifically affects the Ca^{2+}-dependent activation pathway associated with D367.

Then, what are the targets in the D367-specific pathway that are subject to modification by mD369G to result in an increase in Ca^{2+} sensitivity? On the basis of the structural model of the RCK1 domain (Jiang et al., 2002), D367 appears to be located some distance from the activation gate. Thus, the D367-specific activation pathway may involve a large structure that includes many residues (Figure 3A). Because mutation mD369G is located close to D367, it is possible that the mutation may alter local interactions of the D369 side chain with the putative Ca^{2+}-binding site to enhance Ca^{2+} sensitivity (Wang et al., 2009). On the other hand, it is also possible that mD369G may alter the conformation of the activation pathway and allosterically enhance Ca^{2+} sensitivity (Figure 2D). To distinguish between these two possibilities, we mutated D369 to conservative (D369E) and neutral (D369A, N, W, and P) amino acids with various side chain sizes and examined the effects of these mutations on Ca^{2+} sensitivity. Among all these mutations, only mD369G increased Ca^{2+} sensitivity, with $V_{1/2}$ of the G-V relations shifted to more negative voltage ranges (Figure 3F). The effects of other mutations were not as pronounced and varied at different $[Ca^{2+}]_i$, increasing channel activation at some concentrations, but decreasing activation at other concentrations. These results suggest that the side chain of D369 is not part of the Ca^{2+}-binding site (also see Shi et al., 2002 and Xia et al., 2002), and it may not contribute to Ca^{2+} sensitivity by the short range electrostatic or van der Waals interactions with the putative Ca^{2+}-binding site. Rather, the specific effect of mD369G in increasing Ca^{2+} sensitivity may derive from the ability of glycine to adopt a wide range of main-chain dihedral angles and make protein structure flexible at its site, which may alter the conformational changes of the D367-specific pathway during channel gating. Consistent with this suggestion, the G-V relation of the mD369G mutant channels shifted a small but significant amount to more negative voltages ($\Delta V_{1/2}$ = 8.8 ± 3.8 mV [mean of difference ± standard error of difference, n = 6 for WT and 20 for mD369G], p = 0.029 in unpaired Student's t test) at 0 $[Ca^{2+}]_i$ (Figure 1E), indicating that mD369G can alter channel function by a change in the structure that links to the activation gate, instead of by merely changing Ca^{2+} binding. Furthermore, although mD369G no longer enhances Ca^{2+} sensitivity of the channel with the D367A mutation, it alters channel activation independently of $[Ca^{2+}]_i$, shifting the G-V relation at all $[Ca^{2+}]_i$ (Figures 3B and 3C). It is possible that D367A eliminated Ca^{2+} binding to the putative site but did not destroy the rest of the activation pathway downstream from Ca^{2+} binding, which was subsequently altered by mD369G mutation to affect channel activation.

To examine whether the flexibility of the channel protein matters to gating and whether mD369G alters the flexibility of the channel protein, we studied the WT and mutant channels in intracellular solutions with increased viscosity. The dynamics of a protein in solution are intimately coupled to the dynamics of the solvent; the fluctuation amplitudes and relaxation rates (i.e., flexibility) of proteins can be reduced by increases in solution viscosity (Ansari et al., 1992; Beece et al., 1980; Frauenfelder et al., 2009). Previous studies showed that the increases in solution viscosity may affect the moving parts of voltage-dependent Na^+ channels during gating to reduce activation rates (Kukita, 1997, 2000). In our experiments, increasing the viscosity of intracellular solution by addition of sucrose (measured viscosity = 0.906 ± 0.003 mPa · s and 23.1 ± 0.1 mPa · s, mean ± SEM, n = 12 at 0 and 2 M sucrose, respectively) slows down the time course of activation and deactivation (Figures 4A and 4B) and enhances Ca^{2+}-dependent activation (Figures 4C and 4D) of both the WT and mD369G channels. At 200 μM $[Ca^{2+}]_i$, the reduction of the deactivation rate is smaller as compared to the enhancement of activation rate (Figure 4B), and because BK channel activation can be approximated by a two-state voltage-dependent activation mechanism at saturating $[Ca^{2+}]_i$ (Cui et al., 1997), the changes in time courses of the current are consistent with the changes in G-V relations. Adding 9 M glycerol in the intracellular solution (measured viscosity = 20.2 ± 0.1 mPa · s, mean ± SEM, n = 12), which resulted in a similar increase of viscosity as 2 M sucrose, also caused similar changes in BK channel activation (Figures 4E and 4F). On the other hand, addition of 2 M urea to intracellular solution, which alters viscosity little (measured viscosity = 0.906 ± 0.003 mPa · s and 0.987 ± 0.005 mPa · s, mean ± SEM, n = 12 at 0 and 2 M urea, respectively), had no effect on channel activation (Figures 4E and 4F), excluding the possibility that the changes in BK channel activation with sucrose were due to changes in osmolarity or other unknown effects associated with high concentrations of solutes. These results suggest that gating of BK channels is affected by the flexibility of the channel protein.

The results show that mutation mD369G alters the responses of activation and deactivation kinetics to the increased viscosity (Figure 4B) and causes a reduced shift of the G-V relation as compared to that in WT when the $[Ca^{2+}]_i$ is increased from 0 to the saturating 200 μM (Figures 4C and 4D). Thus, the enhancement of Ca^{2+} sensitivity due to an increase of viscosity for mD369G channels is less than that for WT. Unlike mD369G, mutation D369A, which does not alter Ca^{2+} sensitivity (Figure 3F), has no effect on the response of BK channels to sucrose (Figure 4D). These results support that mD369G alters the flexibility of the BK channel protein to potentiate Ca^{2+} sensitivity.

Results in Figure 3 have shown that mD369G specifically alters the Ca^{2+}-dependent activation pathway associated with D367 (Figure 3C), but not the pathway associated with the Ca^{2+} bowl (Figure 3E). Our unpublished results also indicate that mD369G does not affect Mg^{2+}-dependent activation (Diez-Sampedro et al., 2006). To examine whether a change of solution viscosity affects any specific metal-dependent activation pathways, we measured channel activation with each of the mutations E374A, D367A, and 5D5N, which abolished metal binding to the Mg^{2+}-binding site (Shi et al., 2002), the Ca^{2+}-binding site at D367 (Shi et al., 2002; Xia et al., 2002), and the Ca^{2+}-binding site at the Ca^{2+} bowl (Schreiber and Salkoff, 1997), respectively. D367A, but not E374A or 5D5N, abolished the response of BK channels to sucrose (Figures 4E and 4F), suggesting that only the Ca^{2+}-dependent activation pathway associated with D367

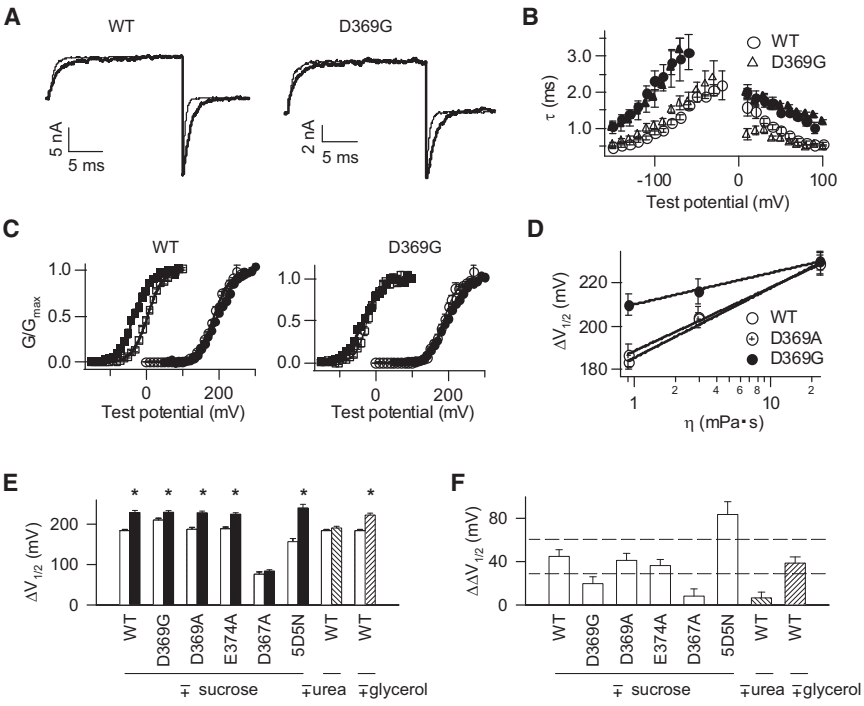

Figure 4. mD369G Mutation Alters Response of BK Channels to Solution Viscosity

(A) Macroscopic current traces recorded in the absence (thinner traces) or presence (thicker traces) of 2 M sucrose. Currents were elicited in saturating 200 μM $[Ca^{2+}]_i$ by 70 mV. Holding and repolarizing voltages were −80 and −120 mV, respectively. Current traces with sucrose were re-scaled to have the same peak amplitude as without sucrose.

(B) Activation (>0 mV) and deactivation (<0 mV) time constant in the absence (hollow symbols) or presence (solid symbols) of 2 M sucrose. $[Ca^{2+}]_i$ = 200 μM. Channels were activated by 70 mV then deactivated by various voltages to obtain deactivation time constant.

(C) G-V curves for WT and mD369G in the absence (hollow symbols) or presence (solid symbols) of 2 M sucrose. $[Ca^{2+}]_i$ = 0 (circles) or 200 μM (squares). Solid lines are fits with the Boltzmann function.

(D) $\Delta V_{1/2}$ versus viscosity. $\Delta V_{1/2} = V_{1/2}$ at 0 $[Ca^{2+}]_i$ − $V_{1/2}$ at 200 μM $[Ca^{2+}]_i$. The solutions contained 0, 1, and 2 M sucrose, respectively. Solid lines are fits with equation $\Delta V_{1/2} = \ln(\eta/\eta_0)^{\gamma}$, where η_0 is the viscosity of zero $\Delta V_{1/2}$ and γ is the slope in the semi-log plot; γ = 13.7 ± 0.9 and 6.2 ± 0.5 (value ± standard deviation) for WT and mD369G, respectively.

(E) $\Delta V_{1/2}$ in the absence (hollow bars) or presence (solid bars) of 2 M sucrose. Hatched bar indicates $\Delta V_{1/2}$ in the presence of 2 M urea or 9 M glycerol. Asterisks indicate a significant difference ($p < 0.05$ in Student's t test) of $\Delta V_{1/2}$ resulted from 2 M sucrose or 9 M glycerol.

(F) $\Delta\Delta V_{1/2}$ caused by sucrose. $\Delta\Delta V_{1/2} = \Delta V_{1/2}{}^{2\text{ M sucrose}} - \Delta V_{1/2}{}^{0\text{ sucrose}}$. Hatched bar indicates $\Delta\Delta V_{1/2}$ caused by 2 M urea or 9 M glycerol. The dashed lines give the 99% confidence interval for $\Delta\Delta V_{1/2}$ of WT.

Error bars represent SEM.

specifically depends on the dynamics of the channel protein for the coupling between Ca^{2+} binding and channel opening, which is consistent with the result that mD369G specifically affects the same activation pathway (Figure 3).

It is important to note that both the increase of viscosity, which reduces the overall protein dynamics, and the mD369G mutation, which enhances the local peptide flexibility, potentiate Ca^{2+} sensing. This result suggests that the local peptide flexibility enhanced by mD369G may reduce the dynamics in other parts of the protein allosterically, consistent with the results in Figures 1E and 3C. Taken together, these results suggest that mD369G alters the flexibility and conformation of the channel protein to potentiate the allosteric coupling between Ca^{2+} binding at the D367 site and channel opening.

Allosteric Interactions in the D367 Pathway

To demonstrate more directly that mD369G affects the allosteric coupling between Ca^{2+} binding and channel opening, we find structural perturbations that affected the coupling in the D367-specific activation pathway and then test whether such perturbations also alter the effect of mD369G. In search of such perturbations, we performed a mutation-scan in the AC region, which is a crucial gateway for the allosteric coupling between Ca^{2+} binding and channel opening because it physically connects the activation gate to the rest of the cytosolic domain (Figure 1A), and is important in determining Ca^{2+} sensitivity (Krishnamoorthy et al., 2005). Furthermore, both the putative Ca^{2+}-binding site D367 and the mutation mD369G are situated within the AC region so that the mutation may alter its structure to affect Ca^{2+} sensitivity. In this experiment, most residues were mutated individually to Ala and some to other amino acids (Figure 5A). The loss of Ca^{2+} sensitivity of the channel due to each mutation is quantified by the change in the G-V shift ($\Delta V_{1/2}$) when $[Ca^{2+}]_i$ changes from nominal 0 to the near saturating 99.3–111.5 μM (i.e., $\Delta\Delta V_{1/2(\Delta Ca^{2+})} = \Delta V_{1/2}{}^{WT} - \Delta V_{1/2}{}^{Mutant}$). We classify a $\Delta\Delta V_{1/2(\Delta Ca^{2+})}$ of more than ± 20 mV as significant because the G-V relation of BK channels often exhibits variations within a voltage range of ≤20 mV. Ten mutations are found to reduce Ca^{2+} sensitivity significantly (indicated by asterisks in Figures 5A and S1, available online), including D362A and D367A, which have been reported elsewhere (Shi et al., 2002; Xia et al., 2002). These mutations are located in different secondary structures within the AC region, including αA, αB, βC, and the interloop between αA and βB that contains Asp-Arg-Asp-Asp at positions 367–370 and is called the DRDD loop (Figure 5A). Consistent with D367 being part of a Ca^{2+}-binding site, mutations in the DRDD loop resulted in large reductions in Ca^{2+} sensitivity; and D367A reduced the G-V shift by 105 ± 4 mV (mean of difference ± standard error of difference, n = 6 for WT and 5 for D367A) as compared to the 182 ± 3 mV (n = 6) total shift in WT mSlo1 in response to an increase of $[Ca^{2+}]_i$ from 0 to 111.5 μM, equivalent to an ~60%

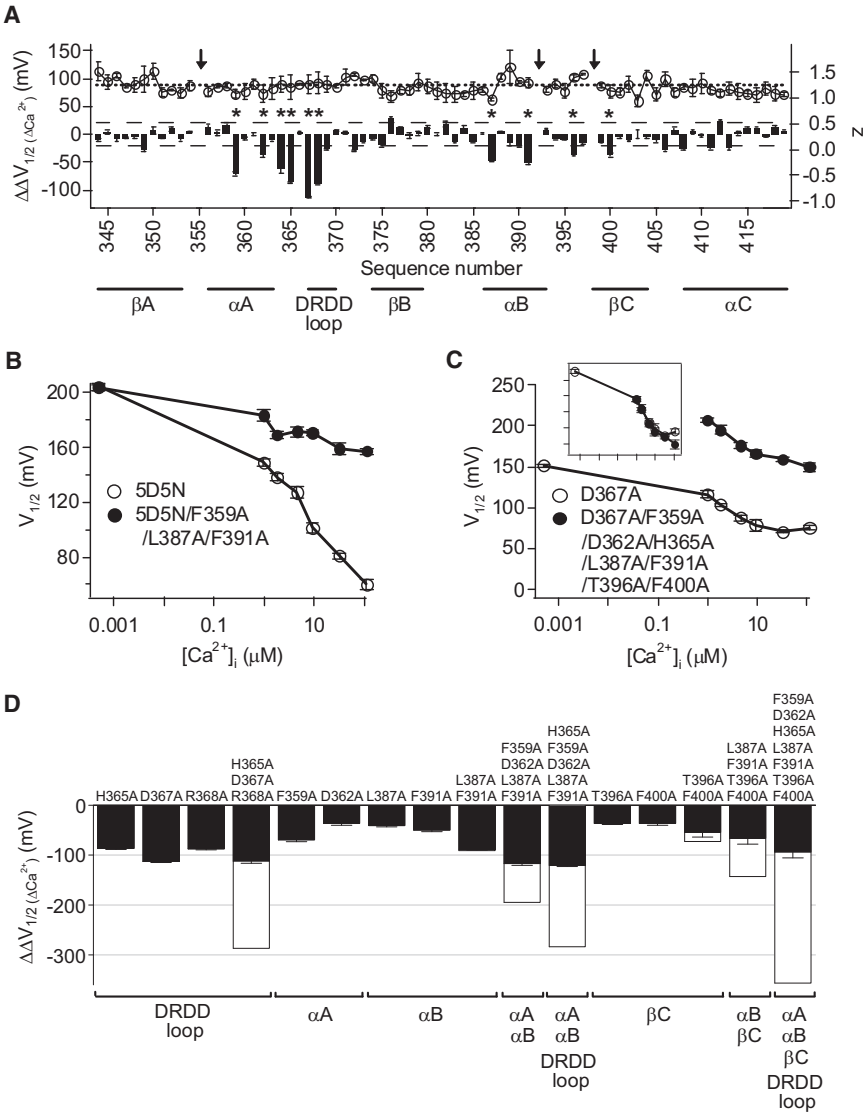

Figure 5. Mutations in the AC Region Perturb the D367-Associated Ca^{2+} Activation Pathway

(A) Effect of the AC region mutations on Ca^{2+} activation. The mutation scan includes H344–A419 of mSlo1 (GenBank accession number, GI: 347143). The residues were individually mutated to Ala except that A389, A412, and A419 were mutated to Gly, Q397 to Cys, and E399 to Asn. $\Delta\Delta V_{1/2(\Delta Ca^{2+})} = \Delta V_{1/2}^{WT} - \Delta V_{1/2}^{Mutant}$, where $\Delta V_{1/2} = V_{1/2}$ at 99.3 to 111.5 μM $[Ca^{2+}]_i - V_{1/2}$ at 0 $[Ca^{2+}]_i$. Mutations with $\Delta\Delta V_{1/2(\Delta Ca^{2+})}$ falling beyond the ± 20 mV (dashed lines) interval significantly affect Ca^{2+} activation, which are (denoted by asterisks) F359A, D362A, L364A, H365A, D367A, R368A, L387A, F391A, T396A, and F400A. Open circles depict z values. The dotted line indicates the z value of WT. Structural motifs are indicated by horizontal thick lines. Arrows indicate mutations from which we were unable to obtain data because either the G-V curves at 0 $[Ca^{2+}]_i$ shifted to extremely positive potentials beyond the range of measurement (S355A and K392A) or the mutant failed to express macroscopic currents (V398A).

(B) $V_{1/2}$ versus $[Ca^{2+}]_i$ for the combined mutation in αA and αB on the background of Ca^{2+} bowl mutation 5D5N.

(C) $V_{1/2}$ versus $[Ca^{2+}]_i$ for the combined mutation in αA, αB, and βC on the background of D367A mutation. The G-V curve at 0 $[Ca^{2+}]_i$ for the combined mutation shifted to extremely positive potentials and hence the $V_{1/2}$ is unavailable. The two curves are shifted vertically to align at 1.0 μM $[Ca^{2+}]_i$ in the inset.

(D) Effect of individual and combined mutations on Ca^{2+} activation (filled bars). Open bars depict the summed effects of individual mutations except for those under F359A/D362A/L387A/F391A and L387A/F391A/T396A/F400A, which show the summed effects of F359A, D362A, and L387A/F391A, and of L387A/F391A and T396A/F400A, respectively. Thick lines indicate the structural motifs where the mutations are located.

Error bars represent SEM.

reduction of Ca^{2+} sensitivity. The functionally important mutations in other secondary structures are separated by large distances from the DRDD loop in the structural model of the RCK1 domain. These residues are important in the D367-specific pathway (see below), but cannot be part of the Ca^{2+}-binding site because of their long distances from D367 and because they are mostly hydrophobic (Figure 5). The long distances from D367 also suggest that it is unlikely for all these residues to make direct interactions with the putative Ca^{2+}-binding site. Therefore, at least some of these mutations reduced Ca^{2+} sensitivity by perturbing the allosteric coupling between Ca^{2+} binding and channel opening.

Because mD369G may enhance Ca^{2+} sensitivity by potentiating the allosteric coupling between Ca^{2+} binding and channel opening, do these perturbations also alter the effect of mD369G? Before answering this question, we examined whether these mutations, like mD369G, are able to affect the activation pathway associated with D367 specifically. Figure 5B shows that the combined mutations in αA and αB with 5D5N (F359A/L387A/F391A/5D5N) reduced Ca^{2+} sensitivity more than 5D5N alone. Because 5D5N completely abolishes the Ca^{2+} sensitivity derived from the Ca^{2+} bowl (Schreiber and Salkoff, 1997; Xia et al., 2002), the additional reduction in Ca^{2+} sensitivity suggests that the mutations in αA and αB may perturb the activation pathway associated with D367. Consistent with these results, the combined mutations in αA, αB, and βC with D367A (F359A/D362A/H365A/L387A/F391A/T396A/F400A/D367A) did not reduce Ca^{2+} sensitivity more than D367A alone (Figure 5C), indicating that these mutations all specifically affect the activation pathway associated with D367; once the upstream pathway is disabled by mutation D367A, additional mutations perturbing the coupling between Ca^{2+} binding and channel opening were no longer able to affect Ca^{2+} sensitivity. With more combinations of mutations, we further studied how these

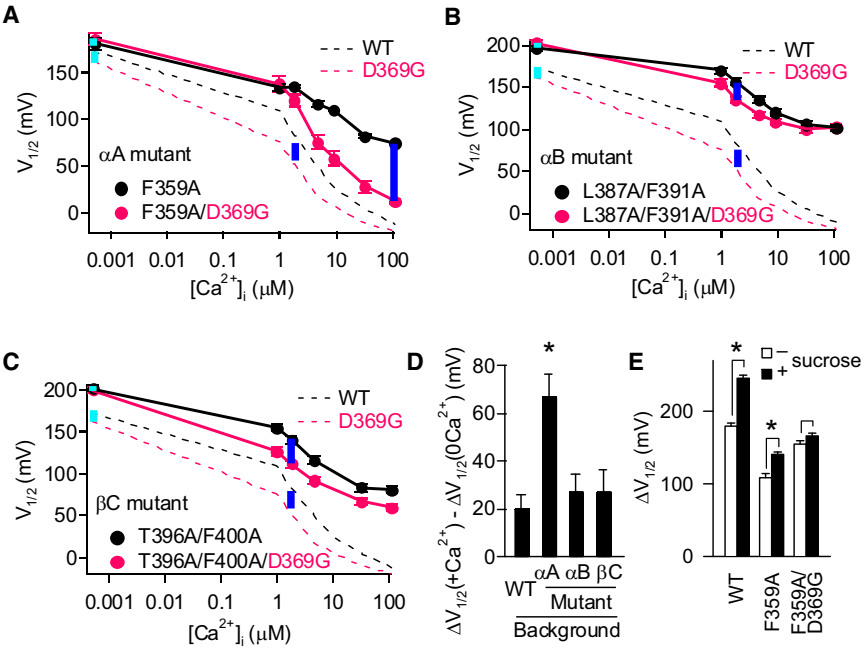

Figure 6. Mutations in the AC Region Allosterically Alter the Effect of mD369G Mutation

(A–C) $V_{1/2}$ versus $[Ca^{2+}]_i$ for the background mutations in αA (A), αB (B), and βC (C) with (red circles) and without (black circles) mD369G, and on the background of WT with (red dashed line) and without (black dashed line) mD369G.

(D) The maximum mD369G-induced increase in Ca^{2+}-dependent activation on the background of WT and mutations. $\Delta V_{1/2}(+Ca^{2+})$ is the maximum $V_{1/2}$ shift caused by mD369G, and measured by the length of the blue lines in (A–C) on respective backgrounds. Note that $\Delta V_{1/2}(+Ca^{2+})$ was measured at 1.8 μM $[Ca^{2+}]_i$ on all backgrounds except for on the background of mutation in αA, where $\Delta V_{1/2}(+Ca^{2+})$ was measured at 111.5 μM $[Ca^{2+}]_i$. $\Delta V_{1/2}(0Ca^{2+})$ is the $V_{1/2}$ shift caused by mD369G at 0 $[Ca^{2+}]_i$, measured by the length of the cyan lines in (A–C). The asterisk indicates that the data is significantly different from that on the WT background ($p < 0.0005$ in unpaired Student's t test).

(E) $\Delta V_{1/2}$ in the absence (hollow bars) or presence (solid bars) of 2 M sucrose. $\Delta V_{1/2} = V_{1/2}$ at 0 $[Ca^{2+}]_i$ − $V_{1/2}$ at 200 μM $[Ca^{2+}]_i$. The asterisk indicates that $\Delta V_{1/2}$ in the presence of sucrose is significantly different from that in the absence of sucrose ($p < 0.05$ in Student's t test).

Error bars represent SEM.

mutations in each individual secondary structure perturb Ca^{2+}-dependent activation (Figures 5D and S2). The Ca^{2+} sensitivity is measured as the total G-V shift induced by a change in $[Ca^{2+}]_i$ from 0 to saturation (Figure 5A), which represents the free energy change during Ca^{2+}-dependent channel opening ($\Delta G_{Ca}{}^{2+} = \Delta zeV_{1/2}$) (Cui and Aldrich, 2000), where *e* is the elementary charge and z is similar at various $[Ca^{2+}]_i$ (Figures 1C and 1D) and largely unchanged by mutations (Figure 5A). Therefore, we assumed that for any combination of mutations, if the mutations do not affect the same molecular process, the sum of the effects on Ca^{2+} sensitivity by the individual mutations should be the same as that of the combined mutations (Horovitz and Fersht, 1990). Mutations in the DRDD loop (H365A/D367A/R368A) reduced Ca^{2+} sensitivity that is indistinguishable from that of the single mutations D367A, indicating that these mutations all affect the same molecular process. Contrarily, the reduction in Ca^{2+} sensitivity was nearly additive by mutations in αB or βC (L387A/F391A or T396A/F400A) (Figure 5D), suggesting that in αB or βC, each mutated amino acid may independently contribute to local interactions that are important for channel gating. However, the combined mutations in αB and βC (L387A/F391A/T396A/F400A) reduced no more or even less Ca^{2+} sensitivity than the mutations in αB alone (L387A/F391A), indicating that αB and βC also cooperate as part of a common molecular process in Ca^{2+}-dependent activation. When the mutations in αA and αB were combined (F359A/D362A/L387A/F391A), they had a larger effect than did mutations in individual secondary structures (F359A, D362A, or L387A/F391A); nonetheless, the effect was less than that of the summed effects of all individual mutations. Therefore, although αA, αB, and βC may be involved in localized interactions, they also cooperate as part of a common molecular process contributing to Ca^{2+}-dependent activation. Taken together, these results suggest that all perturbations in the AC region that reduce Ca^{2+} sensitivity (Figure 5A) affect the activation pathway associated with D367, and they all are allosterically connected such that one perturbation can affect the outcome of other perturbations.

mD369G Alters Allosteric Interactions

We then examined how the above mutations alter the effect of mD369G by combining mD369G with mutations in αA (F359A), αB (L387A/F391A) or βC (T396A/F400A) that are likely to be located long distances away from D369 (Figure 6). Interestingly, although the mutations in αA, αB, or βC reduce total Ca^{2+} sensitivity, they either enhanced or did not significantly alter the effect of mD369G (Figures 6A–6D). Compared to the WT mSlo1, the mD369G mutation shifted the G-V relation maximally around 1.8 μM $[Ca^{2+}]_i$; however, the mutation in αA altered the profile of mD369G effects and increased G-V shift, with the largest shift at 111.5 μM $[Ca^{2+}]_i$ (Figures 6A and 6D). The mutations in αB or βC did not alter the profile of mD369G effects or the maximal G-V shifts (Figures 6B–6D). Thus, the effect of mD369G is determined by the mutations in αA, αB, and βC within the AC region. Because these mutations are all allosterically connected in perturbing the D367-specific Ca^{2+}-dependent activation pathway (Figure 5), any of these mutations would alter most allosteric interactions within the AC region to provide a unique network of allosteric connections that determines the effects of mD369G on Ca^{2+} sensitivity. Reciprocally, mD369G also affects most allosteric interactions in the AC region to enhance Ca^{2+} sensitivity. Figure 6E shows that, in the presence of F359A, mD369G reduced the response of channel activation to the

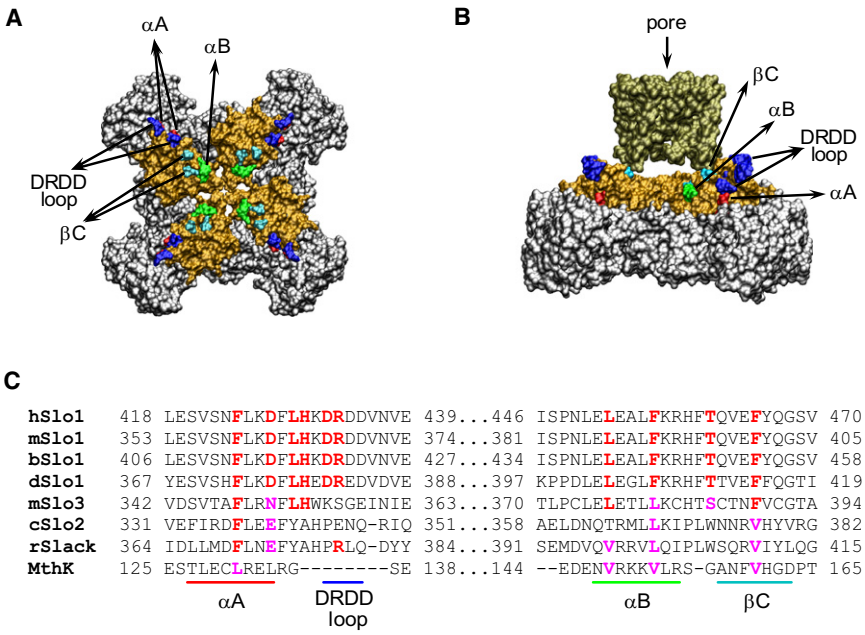

Figure 7. Spatial Distribution and Conservation of the Residues Important for Ca^{2+}-Dependent Activation

(A and B) The structure of the MthK gating ring (gray) superimposed with the homology model of the BK channel AC region (orange) either without (A, top view) or with (B, side view) the pore domain of the BK channel (olive). The pore domain of the BK channel is modeled by using Kv1.2 crystal structure as the template. The residues identified in Figure 5A as being important for Ca^{2+}-dependent activation are marked with blue, red, green, and cyan colors in the structure.

(C) Sequence alignment for the structural motifs in the AC region of Slo and MthK channels. The residues identical to those identified in Figure 5A as being important for Ca^{2+}-dependent activation are in red, and the conserved residues are in purple. The structural motifs are indicated by horizontal lines. BK channels from different species are shown: hSlo1, human (GenBank accession number, GI: 26638649); mSlo1, mouse (347143); bSlo1, bovine (46396286); dSlo1, *Drosophila* (7301192). Also shown are mSlo3, the pH-sensitive mouse Slo3 channel (6680542); cSlo2, the Cl^--sensitive *C. elegans* Slo2 channel (5764632); rSlack, the Na^+ sensitive rat Slack channel (3978471); and MthK (2622639).

increase of viscosity, suggesting that F359A does not alter the mechanism for the function of mD369G such that mD369G may still reduce the flexibility of the AC region even though the allosteric pathway is altered by F359A. On the basis of all the results presented in this article, we conclude that mD369G alters the conformation and dynamics of the channel protein allosterically to potentiate Ca^{2+} sensing via the pathway associated with D367, and the AC region is an important structural component of this pathway.

DISCUSSION

This study demonstrates that mD369G enhances BK channel activity by altering the allosteric coupling between Ca^{2+} binding and gate opening. The experimental results that lead to this conclusion have also brought insights into the mechanism of such a coupling. Previous studies suggested that Ca^{2+} binds to two putative sites, the D367 site (Xia et al., 2002) and the Ca^{2+} bowl (Schreiber and Salkoff, 1997), in BK channels to activate the channel through two separate intramolecular pathways (i.e., two separate subsets of conformational changes are responsible for coupling the activation gate to the two Ca^{2+}-binding sites). However, aside from the putative Ca^{2+}-binding sites, the structural basis of the two activation pathways was not clear. In this study, we show that the mD369G mutation and the mutations in the AC region primarily alter the Ca^{2+} dependence derived from the D367-associated activation pathway (Figures 3, 4, and 6). These results further demonstrate that Ca^{2+} activates the channel through separate intramolecular pathways, and the allosteric interactions within the AC region are part of the D367-specific pathway.

Our results suggest that the AC region is an important structural component in coupling Ca^{2+} binding to channel opening. Consistent with this role, homology modeling of the AC region in BK channels and its superimposition on the full gating ring of the MthK channel reveal that the Ca^{2+}-sensitive mutations are distributed in a distinct fashion from the periphery of the cytosolic domain to the center of the channel (Figures 7A and 7B). The DRDD loop, where the putative Ca^{2+}-binding site and the mD369G mutation are located, is positioned at the outer edge of the channel molecule, and αA, αB, and βC lie just beneath the central pore, making it possible for the allosteric connection within the AC region to couple Ca^{2+} binding to the activation gate. Sequence alignments show that the residues important for Ca^{2+} sensitivity in the AC region are conserved among Slo1 channels from fruit fly to human (Figure 7C), suggesting that all BK channels may share the same Ca^{2+} activation mechanism. Interestingly, although the DRDD loop is highly conserved among the Ca^{2+}-activated Slo1 channels, other Slo families that are activated by intracellular H^+ (Schreiber et al., 1998), Na^+ (Yuan et al., 2003), and/or Cl^- (Yuan et al., 2000) ions show variations in this region (Figure 7C). In addition, this loop is not present in the prokaryotic MthK or the *Escherichia coli* K^+ channels (Jiang et al., 2002; Jiang et al., 2001). Therefore, the residues in the Slo1 DRDD loop appear to be specifically important for Ca^{2+} sensing. In contrast, the sequences of αA, αB, and βC are highly conserved among all Slo families. The residues corresponding to F359, L387, F391, T396, and F400 in mSlo1 are hydrophobic in these channels, and the residues corresponding to D362 are either negatively charged or polar. These comparisons suggest a common role for αA, αB, and βC in the gating mechanism of eukaryotic channels that are sensitive to intracellular ions. It is possible that, in all these channels,

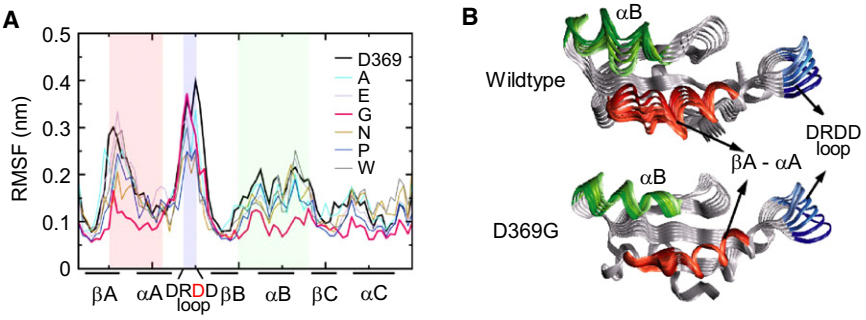

Figure 8. mD369G Mutation Reduces the Flexibility of the AC Region in Molecular Dynamics Simulations

(A) RMS fluctuation of C_α concentrations in the AC region obtained from molecular dynamics simulations of WT and D369A, E, G, N, P and W. Color shades indicate the structural motifs in the AC region, the dynamics of which are significantly affected by mD369G.

(B) Motion of the WT (top) and mD369G (bottom) AC regions along the principal eigenvector from minima to maxima. Color codes are the same as in (A).

αA, αB, and βC modulate gate opening, but the modulation is allosterically controlled by various intracellular ions that specifically bind to their respective binding sites. A change in this allosteric mechanism such as the hD434G mutation can alter the function of these channels and result in human diseases.

An increase of viscosity in intracellular solutions enhances Ca^{2+} sensitivity of BK channels, suggesting that the dynamics of the channel protein is important in the allosteric pathway associated with D367. Two lines of evidence indicate that mD369G alters the dynamics of the channel protein to potentiate Ca^{2+} sensing, namely mD369G, but not other mutations of D369, enhances Ca^{2+} sensitivity (Figure 3F) and alters the responses of the channel to changes in solution viscosity (Figure 4D). To explore the possible mechanisms of how mD369G changes channel function, we performed molecular dynamics (MD) simulations for the AC region. Previous studies have suggested that the AC region may form an independent structural and functional unit in BK channels. First, it was demonstrated that a cleavage at 12 amino acids after the AC region does not prevent the resulting two divided peptides from forming functional channels, suggesting that the cytosolic domain in the N-terminal part of the divided Slo1 may be able to fold independently (Pico, 2003). Therefore, as the core of this cytosolic domain, the AC region may be treated as a structural unit in MD simulations. Second, we previously found that the entire AC region, but not any part of it, was responsible for the Ca^{2+} sensitivity difference between two Slo1 homologs, suggesting that the AC region also acted as a functional unit to modulate Ca^{2+} sensitivity (Krishnamoorthy et al., 2005). This idea is also supported by the results that mutations within the AC region are allosterically connected in perturbing Ca^{2+} sensitivity (Figure 5).

Figure 8A plots root mean square fluctuation (RMSF) of the main chain C_α concentrations for the AC regions of the WT and mD369G mSlo1, as well as the AC regions of mutations D369E, A, N, W, and P that have little effect on Ca^{2+} sensitivity (Figure 3F). RMSF is the standard deviation of the movement of a residue around its mean position (i.e., residues with a higher RMSF are in a more flexible region of the protein). Consistent with the experimental data (Figures 1E, 3C, 3F, 4, and 6A–6D), mutation mD369G not only alters the local flexibility but also changes the overall dynamics of the AC region. The changes are most prominent in three areas of the AC region; the peak RMSF shifts in the DRDD loop and the maximum differences occur in the βA-αA linker and αB-βC (red, blue, and green shades, Figure 8A), corresponding to the same areas where the mutations reduce Ca^{2+} sensitivity with allosteric connections (Figure 5). Also correlating with the experimental results of channel activation (Figures 3F, 4E, and 4F), the dynamics of the D369E, A, N, W, and P mutant AC regions do not show similar changes as that of mD369G. For a better visualization, the changes in dynamics caused by mD369G are also illustrated by decomposing the complex motion into simpler periodic orthogonal modes using principal component analysis and plotting the movements of the most significant mode (Figure 8B). The overall effect of mD369G is to reduce the flexibility in the βA-αA linker and αB-βC, causing the entire AC region to move as a more rigid entity that simply follows the motion of the DRDD loop (Figure 8B and Movie S1, available online), consistent with the result that both mD369G and an increase of solution viscosity enhances Ca^{2+} sensing (Figures 1 and 4). It is remarkable that the results of MD simulation and experiments correlate well in almost every aspect, although the structure of the AC region is based on a homology model derived from the structure of MthK. This result is consistent with a number of previous studies that demonstrated the structural homology between the RCK1 domain in BK channels and the RCK domain of MthK (Cui et al., 2009; Wang and Sigworth, 2009). Thus, the MD simulation shows a plausible mechanism for mD369G to change the dynamics of the channel protein, which affects the allosteric coupling in the D367 activation pathway by altering the traverse of a dynamic substates ensemble or entropy in the free energy of channel gating (Kern and Zuiderweg, 2003; Popovych et al., 2006).

This dynamic-based allosteric mechanism can be an important target for BK channel modulation. For instance, reported values of intracellular viscosity range from 1 mPa · s (the viscosity of pure water) to >100 mPa · s (Kuimova et al., 2009; Wandelt et al., 2005). Such a variation may be due to different samples and techniques of measurements as well as physiological states of the cell (Kuimova et al., 2009). Within this range of viscosity, Ca^{2+} sensitivity of WT BK channels increases with viscosity and can be equivalent or even larger than that of mD369G channels (Figure 4D). These results reveal a possibility that, at certain physiological states, a high intracellular viscosity could be associated with epilepsy by altering the protein dynamics and potentiating Ca^{2+} sensitivity of BK channels. On the other hand, a reduction of intracellular viscosity reduces Ca^{2+} sensitivity of the mD369G mutant channels (Figure 4D), which may prevent the role of this mutation in epilepsy. These possibilities need to be explored by future investigations.

EXPERIMENTAL PROCEDURES

Mutagenesis and Expression

The mutations were made using overlap-extension PCR from the *mbr5* splice variant of mSlo1(GenBank accession number, GI: 347143) (Butler et al., 1993). The PCR-amplified regions of all the mutations were verified by sequencing. RNA was transcribed in vitro with T3 polymerase (Ambion, TX) and injected into *Xenopus laevis* oocytes (stage V–VI) with an amount of 0.05–50 ng each, followed by 2–5 days of incubation at 18°C.

Electrophysiology

Inside-out patches were formed from oocyte membrane by borosilicate pipettes of 0.8–1.5 MΩ resistance. Macroscopic currents were recorded with an Axopatch 200-B patch clamp amplifier (Axon Instruments, CA) and PULSE acquisition software (HEKA Electronik, Germany). The current signals were low-pass-filtered at 10 kHz with the amplifier's four-pole Bessel filter and digitized at 20-μs intervals. The pipette solution contains 140 mM potassium methanesulphonic acid, 20 mM HEPES, 2 mM KCl, and 2 mM $MgCl_2$ (pH 7.2). The nominal 0 μM $[Ca^{2+}]_i$ solution contains 140 mM potassium methanesulphonic acid, 20 mM HEPES, 2 mM KCl, 5 mM EGTA, and 22 mg/L (+)-18-crown-6-tetracarboxylic acid (18C6TA) (pH 7.2). The free $[Ca^{2+}]$ in the nominal 0 $[Ca^{2+}]_i$ solution is about 0.5 nM. $CaCl_2$ was added to a solution containing 140 mM potassium methanesulphonic acid, 20 mM HEPES, 2 mM KCl, 1 mM EGTA, and 22 mg/L 18C6TA (pH 7.2) to obtain the desired free $[Ca^{2+}]$, which was measured by a Ca^{2+}-sensitive electrode (Thermo Electron, MA). In experiments that changed viscosity, sucrose, glycerol, or urea was added to either the nominal 0 μM $[Ca^{2+}]_i$ solution or the solution containing 200 μM free $[Ca^{2+}]$ which is composed of 140 mM potassium methanesulphonic acid, 20 mM HEPES, 2 mM KCl, and 0.2 mM $CaCl_2$ (pH 7.2). Free $[Ca^{2+}]$ (200 μM) was used to ensure a saturating binding of Ca^{2+} to the channels. Viscosity was measured using a Brookfield DV-III ULTRA Programmable Rheometer (Brookfield Engineering Laboratories, MA) with a model 40 spindle. Viscosity was measured under two spindle rotation rates, 30 and 60 RPM, except for solutions with 2 M sucrose or 9 M glycerol, of which the viscosity was measured under 6 and 12 RPM. All the solutions are Newtonian fluids so that the viscosity does not change with spindle rotation rate. All the experiments were performed at room temperature (22°C –24°C).

Analysis

The tail current amplitudes at −50 mV were measured to determine the relative conductance. The conductance–voltage (G–V) curves were fitted with the Boltzmann function:

$$\frac{G}{G_{max}} = \frac{1}{1+\exp\left(-\frac{ze(V-V_{1/2})}{kT}\right)}$$

where G/G_{max} is the ratio of conductance to maximal conductance, z is the number of equivalent charges, e is the elementary charge, V is membrane potential, $V_{1/2}$ is the voltage where G/G_{max} reaches 0.5, k is Boltzmann's constant, and T is absolute temperature. Error bars in this article represent standard error of means (SEM).

Monod-Wyman-Changeux (MWC) Model

MWC model fits use the following equation:

$$P_{open} = \frac{1}{1+L(0)\cdot e^{\frac{-zeV}{kT}}\cdot\left[\frac{1+\frac{[Ca^{2+}]}{K_C}}{1+\frac{[Ca^{2+}]}{K_O}}\right]^4}$$

where P_{open} is channel's open probability; $L(0)$ is the equilibrium-state ratio of closed to open channels ([C]/[O]) in the absence of bound Ca^{2+} at 0 mV; z, e, V, k, and T are the same as above in Boltzmann function; and K_c and K_o are the dissociation constants of Ca^{2+} in the closed and open states, respectively.

Ca^{2+} Sensitivity by Limiting Slope Measurement

The limiting slope measurement is applied to determine the open probability at extremely negative voltages (Horrigan et al., 1999). The open probability determined by limiting slope measurement is combined with the corresponding G-V relation to construct a P_o-V curve, which is fitted to the following HCA model (Horrigan et al., 1999):

$$P_o = \frac{1}{1+\frac{\exp\left(-\frac{z_L FV}{RT}\right)}{L_o}\left(\frac{1+\exp\left(\frac{z_J F(V-V_{hc})}{RT}\right)}{1+\exp\left(\frac{z_J F(V-V_{ho})}{RT}\right)}\right)^4}$$

where z_L is the charge associated with gate opening when all the voltage sensors are at their resting state. z_J is the charge associated with voltage sensor movements. L_0 is the intrinsic open probability at $V = 0$ while all the voltage sensors are at their resting state. V_{hc} and V_{ho} are the voltages for half of the voltage sensors to be at their activation state at the closed and the open conformations, respectively. All the fittings have fixed $z_L = 0.1$, $z_J = 0.57$, and $V_{hc} = 172$ mV; L_0 and V_{ho} are optimized for the best fitting to reflect the Ca^{2+} dependence (Horrigan and Aldrich, 2002).

In Figures 2B and 2C, the P_o at −140 mV is obtained from the HCA model fittings, which is more accurate than that from direct measurements because the model fittings take into account all the P_o-V data at a certain $[Ca^{2+}]_i$ to eliminate experimental variations.

Homology Modeling

Sequence alignment of mSlo1 (GenBank accession number, GI: 347143) with MthK channel (1LNQ, GI: 2622639) and Kv1.2 channel (2A79, GI: 1235594) was performed using ClustalW (Thompson et al., 1994). The gaps in the sequence were predicted using the Protein Loop Optimization Algorithm (PLOP) (Jacobson et al., 2004). Homology models of the mSlo1 AC region (Gly341-Asp420) were generated using Modeler (Sali and Blundell, 1993).

Molecular Dynamics Simulations

The package GROMACS (Lindahl et al., 2001) was used for all MD simulations. The simulations were performed at 300 K using an NpT ensemble, OPLS/AA force field, and explicit SPC solvent. In all cases, 2 fs time steps were used along with periodic boundary conditions, hydrogen bond constraints, and Particle Mesh Ewald for the calculation of long-range electrostatics. The protocol for the simulation involved energy minimization, followed by heating to 300 K at intervals of 50 K, equilibration for 40 ps, and finally the 80 ns production run. The coordinates were saved every 50 ps for subsequent analysis. The 80 ns simulation is limited by computation capacities and is shorter than the timescale of BK channel gating that is at ~0.1 ms. Nevertheless, motions of the backbone on the ps–ns timescale have been shown experimentally as an important carrier of allosteric energy (Kern and Zuiderweg, 2003; Popovych et al., 2006).

Root Mean Square Fluctuations

The root mean squared fluctuation of every atom was found using the formula

$$\mathrm{RMSF} = \sqrt{\frac{1}{N}\sum\left(x_i - \langle x_i\rangle\right)^2}$$

where x_i is the position of atom i in each simulation frame and $\langle x_i\rangle$ is the average of x over all frames.

Principal component analysis

The trajectory obtained from our MD simulations was decomposed into orthogonal modes and the motion of the protein along the first few modes was studied. C_{ij}, the correlation between the movement of an atom i and atom j was found for all N C_α atoms of the protein to form an N*N covariance matrix. $C_{ij} = \langle M_{ii}^{1/2}(x_i - \langle x_i\rangle)M_{jj}^{1/2}(x_j - \langle x_j\rangle)\rangle$, where M is a diagonal matrix containing the masses of the atoms. The covariance matrix was diagonalized to get N eigenvectors and corresponding eigenvalues. The MD trajectory was projected on the eigenvector having the largest eigenvalue to get the principal mode that captures the largest amplitude motion of the protein.

SUPPLEMENTAL INFORMATION

Supplemental Information for this article includes one figure and one movie and can be found with this article online at doi:10.1016/j.neuron.2010.05.009.

ACKNOWLEDGMENTS

We thank Frank Horrigan, Toshi Hoshi, Urvi Lee, Lawrence Salkoff, and Chris Lingle for helpful suggestions. We thank Dr. Jin-Yu Shao for allowing us to use the Rheometer. The mSlo1 clone was kindly provided by Lawrence Salkoff (Washington University, St. Louis, MO). This work was supported by National Institutes of Health (grant R01-HL70393 to J.C.). J.C. is an Associate Professor of Biomedical Engineering on the Spencer T. Olin Endowment.

G.K. and J.C. initiated the study. G.K., J.Y., G.Z., and J.C. made key experimental observations. A.S. and D.S. performed molecular modeling and MD simulations, which provided motivation for experiments in Figure 5. G.K., J.Y., and J.S. performed experiments in Figures 1, 3, and 5. J.Y. and J.S. performed experiments in Figures 2, 4, and 6. G.Z., H.Y., and K.D. also performed experiments in Figures 1 and 5. J.Y., G.K., A.S., and J.C. wrote the manuscript, with revisions from H.Y. and D.S.

Accepted: May 3, 2010
Published: June 23, 2010

REFERENCES

Ansari, A., Jones, C.M., Henry, E.R., Hofrichter, J., and Eaton, W.A. (1992). The role of solvent viscosity in the dynamics of protein conformational changes. Science *256*, 1796–1798.

Ashcroft, F.M. (2000). Ion Channels and Disease: Channelopathies (San Diego, California, USA: Academic Press).

Atkinson, N.S., Robertson, G.A., and Ganetzky, B. (1991). A component of calcium-activated potassium channels encoded by the *Drosophila slo* locus. Science *253*, 551–555.

Beece, D., Eisenstein, L., Frauenfelder, H., Good, D., Marden, M.C., Reinisch, L., Reynolds, A.H., Sorensen, L.B., and Yue, K.T. (1980). Solvent viscosity and protein dynamics. Biochemistry *19*, 5147–5157.

Bezanilla, F. (2008). How membrane proteins sense voltage. Nat. Rev. Mol. Cell Biol. *9*, 323–332.

Brenner, R., Chen, Q.H., Vilaythong, A., Toney, G.M., Noebels, J.L., and Aldrich, R.W. (2005). BK channel [beta]4 subunit reduces dentate gyrus excitability and protects against temporal lobe seizures. Nat. Neurosci. *8*, 1752–1759.

Butler, A., Tsunoda, S., McCobb, D.P., Wei, A., and Salkoff, L. (1993). mSlo, a complex mouse gene encoding "maxi" calcium-activated potassium channels. Science *261*, 221–224.

Cox, D.H., Cui, J., and Aldrich, R.W. (1997). Allosteric gating of a large conductance Ca-activated K^+ channel. J. Gen. Physiol. *110*, 257–281.

Cui, J., and Aldrich, R.W. (2000). Allosteric linkage between voltage and Ca^{2+}-dependent activation of BK-type mslo1 K^+ channels. Biochemistry *39*, 15612–15619.

Cui, J., Cox, D.H., and Aldrich, R.W. (1997). Intrinsic voltage dependence and Ca^{2+} regulation of *mslo* large conductance Ca-activated K^+ channels. J. Gen. Physiol. *109*, 647–673.

Cui, J., Yang, H., and Lee, U. (2009). Molecular mechanisms of BK channel activation. Cell. Mol. Life Sci. *66*, 852–875.

Diez-Sampedro, A., Silverman, W.R., Bautista, J.F., and Richerson, G.B. (2006). Mechanism of increased open probability by a mutation of the BK channel. J. Neurophysiol. *96*, 1507–1516.

Du, W., Bautista, J.F., Yang, H., Diez-Sampedro, A., You, S.-A., Wang, L., Kotagal, P., Luders, H.O., Shi, J., Cui, J., et al. (2005). Calcium-sensitive potassium channelopathy in human epilepsy and paroxysmal movement disorder. Nat. Genet. *37*, 733–738.

Frauenfelder, H., Chen, G., Berendzen, J., Fenimore, P.W., Jansson, H., McMahon, B.H., Stroe, I.R., Swenson, J., and Young, R.D. (2009). A unified model of protein dynamics. Proc. Natl. Acad. Sci. USA *106*, 5129–5134.

Horovitz, A., and Fersht, A.R. (1990). Strategy for analysing the co-operativity of intramolecular interactions in peptides and proteins. J. Mol. Biol. *214*, 613–617.

Horrigan, F.T., and Aldrich, R.W. (2002). Coupling between voltage sensor activation, Ca^{2+} binding and channel opening in large conductance (BK) potassium channels. J. Gen. Physiol. *120*, 267–305.

Horrigan, F.T., Cui, J., and Aldrich, R.W. (1999). Allosteric voltage gating of potassium channels I. Mslo ionic currents in the absence of Ca^{2+}. J. Gen. Physiol. *114*, 277–304.

Jacobson, M.P., Pincus, D.L., Rapp, C.S., Day, T.J., Honig, B., Shaw, D.E., and Friesner, R.A. (2004). A hierarchical approach to all-atom protein loop prediction. Proteins *55*, 351–367.

Jiang, Y., Lee, A., Chen, J., Cadene, M., Chait, B.T., and MacKinnon, R. (2002). Crystal structure and mechanism of a calcium-gated potassium channel. Nature *417*, 515–522.

Jiang, Y., Pico, A.R., Cadene, M., Chait, B.T., and MacKinnon, R. (2001). Structure of the RCK domain from the *E. coli* K^+ channel and demonstration of its presence in the human BK channel. Neuron *29*, 593–601.

Kern, D., and Zuiderweg, E.R. (2003). The role of dynamics in allosteric regulation. Curr. Opin. Struct. Biol. *13*, 748–757.

Krishnamoorthy, G., Shi, J., Sept, D., and Cui, J. (2005). The NH_2 terminus of RCK1 domain regulates Ca^{2+}-dependent BK_{Ca} channel gating. J. Gen. Physiol. *126*, 227–241.

Kuimova, M.K., Botchway, S.W., Parker, A.W., Balaz, M., Collins, H.A., Anderson, H.L., Suhling, K., and Ogilby, P.R. (2009). Imaging intracellular viscosity of a single cell during photoinduced cell death. Nat. Chem. *1*, 69–73.

Kukita, F. (1997). Solvent-dependent rate-limiting steps in the conformational change of sodium channel gating in squid giant axon. J. Physiol. *498*, 109–133.

Kukita, F. (2000). Solvent effects on squid sodium channels are attributable to movements of a flexible protein structure in gating currents and to hydration in a pore. J. Physiol. *522*, 357–373.

Lindahl, E., Hess, B., and van der Spoel, D. (2001). GROMACS 3.0: a package for molecular simulation and trajectory analysis. J. Mol. Model. *7*, 306–317.

Long, S.B., Campbell, E.B., and MacKinnon, R. (2005). Crystal structure of a mammalian voltage-dependent shaker family K^+ channel. Science *309*, 897–903.

Magleby, K.L. (2003). Gating mechanism of BK (Slo1) channels: so near, yet so far. J. Gen. Physiol. *121*, 81–96.

Niu, X., Qian, X., and Magleby, K.L. (2004). Linker-gating ring complex as passive spring and Ca^{2+}-dependent machine for a voltage- and Ca^{2+}-activated potassium channel. Neuron *42*, 745–756.

Pico, A.R. (2003). RCK domain model of calcium activation in BK channels. PhD Thesis, The Rockefeller University.

Popovych, N., Sun, S., Ebright, R.H., and Kalodimos, C.G. (2006). Dynamically driven protein allostery. Nat. Struct. Mol. Biol. *13*, 831–838.

Qian, X., Niu, X., and Magleby, K.L. (2006). Intra- and intersubunit cooperativity in activation of BK channels by Ca^{2+}. J. Gen. Physiol. *128*, 389–404.

Sali, A., and Blundell, T.L. (1993). Comparative protein modelling by satisfaction of spatial restraints. J. Mol. Biol. *234*, 779–815.

Schreiber, M., and Salkoff, L. (1997). A novel calcium-sensing domain in the BK channel. Biophys. J. *73*, 1355–1363.

Schreiber, M., Wei, A., Yuan, A., Gaut, J., Saito, M., and Salkoff, L. (1998). Slo3, a novel pH-sensitive K^+ channel from mammalian spermatocytes. J. Biol. Chem. *273*, 3509–3516.

Schreiber, M., Yuan, A., and Salkoff, L. (1999). Transplantable sites confer calcium sensitivity to BK channels. Nat. Neurosci. *2*, 416–421.

Shen, K.Z., Lagrutta, A., Davies, N.W., Standen, N.B., Adelman, J.P., and North, R.A. (1994). Tetraethylammonium block of *Slowpoke* calcium-activated

potassium channels expressed in *Xenopus* oocytes: evidence for tetrameric channel formation. Pflugers Arch. *426*, 440–445.

Shi, J., Krishnamoorthy, G., Yang, Y., Hu, L., Chaturvedi, N., Harilal, D., Qin, J., and Cui, J. (2002). Mechanism of magnesium activation of calcium-activated potassium channels. Nature *418*, 876–880.

Swartz, K.J. (2008). Sensing voltage across lipid membranes. Nature *456*, 891–897.

Sweet, T.-B., and Cox, D.H. (2008). Measurements of the BK_{Ca} channel's high-affinity Ca^{2+} binding constants: effects of membrane voltage. J. Gen. Physiol. *132*, 491–505.

Thompson, J.D., Higgins, D.G., and Gibson, T.J. (1994). CLUSTAL W: improving the sensitivity of progressive multiple sequence alignment through sequence weighting, position-specific gap penalties and weight matrix choice. Nucleic Acids Res. *22*, 4673–4680.

Unwin, N. (2003). Structure and action of the nicotinic acetylcholine receptor explored by electron microscopy. FEBS Lett. *555*, 91–95.

Wandelt, B., Cywinski, P., Darling, G.D., and Stranix, B.R. (2005). Single cell measurement of micro-viscosity by ratio imaging of fluorescence of styrylpyridinium probe. Biosens. Bioelectron. *20*, 1728–1736.

Wang, B., Rothberg, B.S., and Brenner, R. (2009). Mechanism of increased BK channel activation from a channel mutation that causes epilepsy. J. Gen. Physiol. *133*, 283–294.

Wang, L., and Sigworth, F.J. (2009). Structure of the BK potassium channel in a lipid membrane from electron cryomicroscopy. Nature *461*, 292–295.

Xia, X.-M., Zeng, X., and Lingle, C.J. (2002). Multiple regulatory sites in large-conductance calcium-activated potassium channels. Nature *418*, 880–884.

Xia, X.M., Fakler, B., Rivard, A., Wayman, G., Johnson-Pais, T., Keen, J.E., Ishii, T., Hirschberg, B., Bond, C.T., Lutsenko, S., et al. (1998). Mechanism of calcium gating in small-conductance calcium-activated potassium channels. Nature *395*, 503–507.

Yang, H., Shi, J., Zhang, G., Yang, J., Delaloye, K., and Cui, J. (2008). Activation of Slo1 BK channels by Mg^{2+} coordinated between the voltage sensor and RCK1 domains. Nat. Struct. Mol. Biol. *15*, 1152–1159.

Yellen, G. (1998). Premonitions of ion channel gating. Nat. Struct. Biol. *5*, 421.

Yuan, A., Dourado, M., Butler, A., Walton, N., Wei, A., and Salkoff, L. (2000). SLO-2, a K^+ channel with an unusual Cl^- dependence. Nat. Neurosci. *3*, 771–779.

Yuan, A., Santi, C.M., Wei, A., Wang, Z.-W., Pollak, K., Nonet, M., Kaczmarek, L., Crowder, C.M., and Salkoff, L. (2003). The sodium-activated potassium channel is encoded by a member of the *slo* gene family. Neuron *37*, 765–773.

Zagotta, W.N., Olivier, N.B., Black, K.D., Young, E.C., Olson, R., and Gouaux, E. (2003). Structural basis for modulation and agonist specificity of HCN pacemaker channels. Nature *425*, 200–205.